J Mater Sci (2008) 43:281–298
DOI 10.1007/s10853-007-2174-9

Vickers indentation behavior of several commercial glasses at high temperatures

Trevor E. Wilantewicz · James R. Varner

Received: 16 July 2007 / Accepted: 17 September 2007 / Published online: 17 October 2007

Abstract The Vickers indentation behavior of five commercial glasses has been investigated as a function of temperature. The glasses included: (i) soda-lime-silica Float glass, (ii) lead-alkali silicate, (iii) 7740 Pyrex™ borosilicate, (iv) potassium phosphate, and (v) lanthanum borate. A recording microindentation system was constructed to allow Vickers indentation testing to be conducted at temperatures significantly above room temperature. The Vickers hardness was observed to decrease continuously with increasing temperature for all glasses, with the exception of the 7740 Pyrex™ glass. Decreases in hardness were attributed to decreases in elastic moduli and bond strength with increasing temperature. The lengths of median-radial cracks around indentations in several glasses were observed to first increase, and then decrease, with increasing temperature. The first of this behavior was attributed to initial increases of the crack driving force, characterized by the quantity (E/H), as well as to a decrease in fracture surface energy. Viscous flow at higher temperatures was believed responsible for a reduction in the crack driving force and crack tip stress, resulting in an eventual decrease in crack length. Viscoelastic behavior of the Float glass was characterized by a rate-dependent hardness and indentation crack pattern. Load–displacement traces indicated an increase in the work of indentation and residual indentation depth with increasing temperature for all glasses.

T. E. Wilantewicz (✉)
Impact Physics Branch, US Army Research Laboratory, ATTN: AMSRD-ARL-WM-TD, Aberdeen Proving Ground, MD 21005, USA
e-mail: twilantewicz@comcast.net

J. R. Varner
Kazuo Inamori School of Engineering, Alfred University, Alfred, NY 14802, USA

Introduction

The forming of many glass products takes place at elevated temperatures where the glass is soft enough to be worked into desired shapes [1, 2]. Even after forming, the temperature of the glass surface may be hot enough such that its surface mechanical properties are different compared to at room temperature. Contact of glass at elevated temperatures can take place with steel rollers, mold surfaces, and possibly small particles stuck to the forming or handling equipment, for example [1, 2]. Glass products may also experience contact at unforeseen elevated temperatures while in service. Since the contact of glass with other objects can introduce surface flaws, it's important to have an understanding of the contact behavior of glass. It is well known that flaws on the surface of glass usually serve as the origins of failure, and are responsible for the low practical strengths of glass [3–5]. Budd et al. [6] have shown the strength of glass bottles contacted at 300 °C by steel to undergo significant strength degradation compared to bottles which were not contacted.

Flaws introduced onto the surface of glass by contact from sharp particles or indenters can significantly degrade its strength and erode away material, as shown by Wiederhorn and Lawn [7], Lawn et al. [8–10], Varner et al. [11], and Ritter et al. [12]. While radial cracks lead to strength degradation because of their near perpendicularity to the surface, lateral cracks lead mainly to erosion of material because of their mostly parallel alignment to the surface [7–9, 11, 12]. These studies also demonstrated that strength degradation of glass occurs when the size of contact-induced flaws become larger and more favorably oriented with respect to the applied stress than the pre-existing flaws on the surface. Most of these studies were conducted at room temperature, although Ritter et al. [12]

conducted some tests at 523 °C. There is a close resemblance of contact damage patterns on glass from sharp indentation [13–15] and that from the impact of sharp particles, which is one reason for the use of indentation testing to study strength degradation of glass.

There have also been studies investigating contact damage of glass at elevated temperature, though not as many as at room temperature. Wiederhorn and Hockey [16] investigated the erosion behavior of soda-lime-silica glass impacted with SiC particles from room temperature up to 680 °C. Although brittle fracture behavior dominated for all temperatures, some viscous relaxation of the glass did take place at the higher temperatures, and which reduced the sizes of the lateral cracks, causing a reduction in erosion rate. In their impact experiments on soda-lime-silica glass at 520 °C, Ritter et al. [12] attributed the decrease in the size of lateral cracks and the higher retained biaxial strength, compared to at 23 °C, to the partial relief of residual stress due to plastic flow of the glass. Westbrook [17] studied the Vickers hardness of several glasses up to 800 °C in a vacuum environment. The glasses included various fused silica, soda-lime-silica glass, and vitreous germania. For the soda-lime-silica and vitreous germania glasses the hardness was observed to decrease more-or-less uniformly with increasing temperature. For the silica glasses the behavior was more varied, and depended on the particular type of silica glass tested. For fused quartz and fused silica the hardness temperature curves showed sudden changes at ~70 °C and ~570 °C. Beginning at ~70 °C the hardness dropped suddenly, and then resumed the more-or-less smooth decrease with temperature until ~570 °C, wherein the hardness rose rapidly. This was followed by a smooth decrease in hardness with increased temperature. Although no explanation for the behavior at ~70 °C was provided, it was suggested that the behavior at ~570 °C was related to the alpha to beta structural transformation found in quartz crystal. Westbrook proposed that some structural remnants from the crystal were carried over to the glass. Quartz crystal tested in the same manner showed a more pronounced increase in hardness at ~570 °C compared to the glassy materials [17].

Keulen and Dissel [18] investigated crack initiation in soda-lime-silica glass submerged in demineralized water at different temperatures using a Vickers diamond indenter. They observed the length of the primary radial cracks increase from ~132 μm to ~156 μm as the temperature increased from 20 °C to 80 °C, respectively. Le Bourhis and Metayer [19] made Vickers indentations in soda-lime-silicate glass (Float glass) from room temperature up to 600 °C in an argon gas environment. The radial crack size and Vickers hardness remained nearly constant from room temperature up to 300 °C. Above 300 °C the Vickers hardness and the radial crack length decreased. This hardness behavior was different from Westbrook's [17] results on soda-lime-silicate glass, which showed the Vickers hardness to decrease with temperature beginning at 20 °C. The authors suggested that at temperatures below 300 °C no viscous relaxation of the glass takes place, but above this temperature viscous relaxation can take place, causing a softening of the glass and a lowering of the hardness [19].

Michel et al. [20] studied the Vickers indentation behavior of soda-lime-silica glass from room temperature up to 400 °C, and found the surface radial crack length to increase with temperature over this range, while the hardness decreased. They attributed the increase in crack length to an increase in the quantity (E/H), with E being Young's modulus and H being Vickers hardness, as the temperature increased. In addition, an increased tendency to form full-penny median cracks as opposed to more surface localized radial (Palmqvist) cracks was observed at 400 °C, compared to at 20 °C for 10 N indentations.

The aim of the current study was to investigate the high-temperature indentation behavior of several glass compositions in detail, including some unique compositions which, to the authors' knowledge, have not been examined in great detail before. Examination of the Vickers hardness, crack size, and indentation morphology as a function of temperature were the primary objectives.

Experimental procedures

High-temperature apparatus

Figure 1 is a schematic of the test system used to study the high-temperature behavior of the glasses. This microindentation system was built and used in a previous study [21] to investigate the room-temperature crack initiation behavior of several of the same glasses tested here; however, several modifications were made for the high-temperature set-up.

A piezoelectric actuator (Model PZL-60, Burleigh Instruments, Inc., Fishers, NY) pushes the Vickers diamond indenter into the sample, which is supported by a ring of ball bearings which rest in a shallow trough on a cylindrical steel holder. A strain gauge load cell (Lebow Model 3189-50, Eaton Corp. Lebow Products, Troy, MI) measures the load as the indenter is pushed in, while two capacitance gauges (Model HPT-40, Capacitec Corporation, Ayer, MA), one on each side of the actuator, monitor the displacement of the indenter via the change in distance between the bottom of the gauges and an aluminum plate located just above the load cell. The load cell had a 22.7 kgf capacity, and the displacement gauges had a total measuring range of 500 μm. Data collection and operation

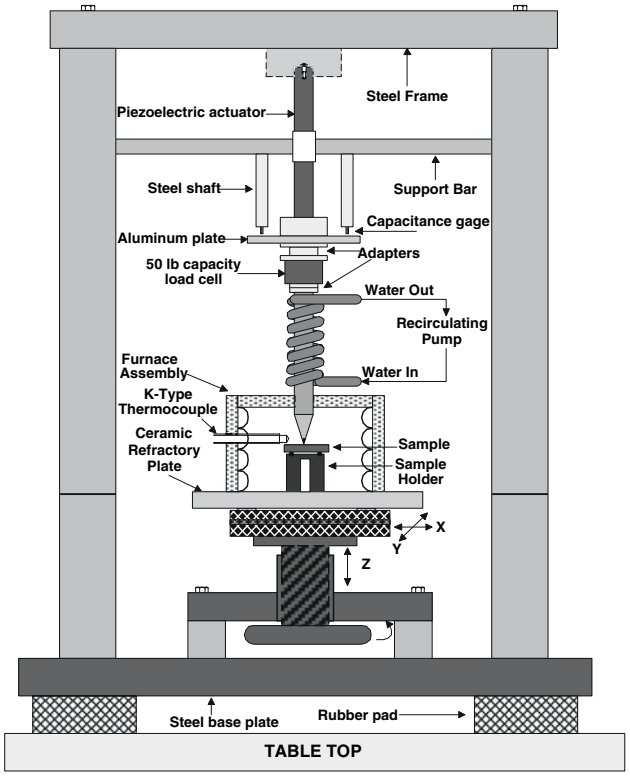

Fig. 1 Schematic of the high-temperature indentation test system

of the instrument were computer controlled. The operator could specify the indenter displacement rate, the maximum load desired, and the hold time at the maximum load. A data acquisition card in the workstation computer collected the load and displacement signals for subsequent analysis. A small circular furnace was built and supported by a flat ceramic refractory plate. The furnace was secured to the refractory plate with high-temperature adhesive. The plate was cemented to metal pegs that were attached to the x-y-z stage of the instrument, which resulted in a rigid mount and no movement of the ceramic plate, and hence furnace, during testing. There was a small gap between the x-y-z stage and the refractory plate which enabled the stage to stay relatively cool and operable during testing. The furnace walls were well insulated with fiber board, while fiber blanket insulated the top of the furnace, and was positioned to allow a small hole for the indenter to pass through. The heating elements were Ni-chrome resistive wire. A K-type thermocouple was positioned inside the furnace, about 3 mm above the specimen surface, to monitor temperature at all times. The furnace was capable of temperatures in excess of 700 °C. The Vickers diamond indenter was attached to a long steel rod, to which hollow copper tubing was attached via solder. A pump re-circulated cold water through the copper tubing, keeping the steel rod near room temperature, and more importantly keeping the output of the load cell stable. An attempt was made to feed a nitrogen gas line into the furnace; however, the rather large hole required to allow the gas to flow into the furnace caused the temperature inside the furnace to fluctuate too much. In addition, since the furnace chamber was relatively small, the cooler nitrogen gas by itself caused the temperature to fluctuate as well. It was therefore decided to test the specimens in laboratory air. Although the oxidation of diamond can be an issue at high temperature, the temperatures in this study were kept below 640 °C. Lu et al. [22] have shown that oxidation of diamond films begins to take place at around 650 °C. In the current study hardness measurements on a steel calibration block both before and after high-temperature testing yielded similar results, and no visible changes in the diamond was noted under an optical microscope after high-temperature testing. In addition, the mass of the indenter both before and after testing at high temperature did not change, indicating no measurable loss of diamond from oxidation.

Sample preparation

The five glass samples were all from commercial glass manufacturers. The Float glass was ~3.2 mm thick and required no polishing. The borosilicate glass was Corning Code 7740 Pyrex™ borosilicate, ~3.4 mm thick, and also required no polishing. Rectangular specimens approximately 30 mm by 25 mm were cut from larger sheets of the Float and Pyrex™ glasses. The three remaining glasses were optical glasses obtained from a commercial glass manufacturer, and are designated as OG1, OG2, and OG3. Rectangular pieces of each glass, approximately 30 mm by 25 mm, and ~3 mm thick, were cut from larger glass blocks, and subsequently polished with diamond solutions down to 1 μm. A final polish using a commercially available cerium oxide polishing compound resulted in very smooth surfaces with few scratches and pits. Multiple specimens were prepared for all five glasses. Prior to testing, all the glasses were annealed at 10 K above their respective glass transition temperatures for 1 h to remove any residual stresses, and then slow cooled at 1 K/min to room temperature. Specimens were then cleaned with reagent grade alcohol and stored in a drying oven kept at 100 °C prior to testing. The glass transition temperatures were provided by the glass manufacturers and are shown in Table 1. Table 2 lists the compositions of the glasses, in mol%. Due to confidentiality concerns, the compositions of the three optical glasses are only approximate, and the actual manufacturer designations of the glasses are not given. OG1 was a lead-alkali-silicate crown glass, OG2 a lanthanum-borate flint glass, and OG3 a

Table 1 Glass transition temperatures (T_g)

Glass	T_g (°C)
Float	554
Pyrex™	560
OG1	459
OG2	642
OG3	520

Table 2 Approximate compositions of glasses (mol%)

	Float	Pyrex™	OG1	OG2	OG3
SiO_2	70.3	81	81		
ZrO_2				6	
Na_2O	13.7	4	6		
K_2O	0.1		5		23
CaO	9.3				
ZnO				5	
PbO			5		
MgO	6.1				
B_2O_3		13		60	
Al_2O_3	0.4	2	5		7
La_2O_3				18	6
Y_2O_3				7	
P_2O_5					64
Nb_2O_5				5	
KHF_2			1		

potassium-phosphate glass used as a host glass in laser applications.

High-temperature testing

Tests were conducted by first placing a glass specimen inside the furnace on top of the sample holder. The furnace was then heated at a rate of 10 K/min until the desired set-point temperature was reached. The specimen was then allowed to equilibrate at the test temperature for anywhere between 30 min and 1 h prior to testing. The temperature stability of the furnace was very good, with readings not fluctuating by more than ±2 °C during testing. The actual temperature was estimated to be accurate to ±4 °C of the set temperature. Indentations were then made on a specimen. Anywhere between 5 and 10 indentations at each temperature were made in different areas of the specimen. A new specimen was used for each temperature investigated, in order to avoid thermal history effects. After testing, the furnace was immediately shut down and the sample was allowed to cool as quickly as possible without cracking. The fiber blanket insulation was partially removed to help allow fast cooling. After the specimen was cool enough to touch, the indentation sites were examined under an optical microscope. The lengths of any median-radial and lateral cracks were measured, as were the indentation diagonal lengths. The Vickers hardness was calculated for each specimen and temperature using the following formula [23]:

$$H_V = \frac{1.8544F}{d^2} \quad (1)$$

where H_V is the Vickers hardness number, F is the indentation load, and d is the average diagonal length, obtained by averaging the two diagonal lengths of an indentation. The Vickers hardness is the load divided by the actual surface area of the indentation, and can be thought to represent a mean contact stress, or pressure. The hardness results were based on anywhere between 3 and 5 indentations. The air side of the Float glass specimen was tested in all experiments. The indentation loads and temperatures used for each specimen varied, and will be made clear in the Results section. The indenter displacement rate also varied, and will be made clear in the Results section. In addition, there was no hold time at the maximum load, i.e., as soon as the maximum load was reached the indenter was withdrawn at the same rate as that used on loading.

Mechanical properties

Measurements were made of the Vickers hardness (H_V), Young's modulus (E), and indentation toughness (K_c) of the five glass samples at room temperature. For Vickers hardness, a standard microhardness tester (HMV-2000, Microhardness Tester, Shimadzu) was used to make 10 indentations per sample at 200 gf load, with a 15 s hold under the maximum load. The hardness was calculated using Eq. 1. Indentation toughness of the samples was calculated according to Eq. 2, after Anstis et al. [24]. Twelve Vickers indentations were made in each sample at loads of either 500 gf or 1,000 gf, and the lengths of the surface traces of the major radial cracks

$$K_c = 0.016\left(\frac{E}{H}\right)^{1/2}\left(\frac{F}{c^{3/2}}\right) \quad (2)$$

were measured immediately after making an indentation, in order to avoid the effects of slow crack growth. All cracks were measured within about 90 s after indentation. In Eq. 2 K_c is toughness, E is Young's modulus, H is hardness, F is indentation load, and c is crack length measured from the center of indentation to the crack tip. The Vickers hardness (H_V) was used for H in Eq. 2. Note that H uses the

projected area, which for a Vickers indenter is $d^2/2$, whereas H_V uses the actual contact area, which is $d^2/1.8544$. The former gives a hardness that is ~8% higher than the latter.

Twelve indentations were made per sample to calculate an average toughness. However, toughness was not measured on the 7740 Pyrex™ glass since this glass densifies significantly under indentation, which invalidates the use of Eq. 2 [14, 24]. For this glass, the toughness was obtained from the work by Wiederhorn [25] on an identically similar composition. Young's modulus and Poisson's ratio (ν) were determined using the pulse-echo time-of-flight technique, where the transit time for shear and longitudinal ultrasonic waves produced by transducers are measured using an oscilloscope. Anywhere between 3 and 5 determinations were made per specimen, and averaged. The equations used to calculate the Young's modulus and Poisson's ratio can be found in the book by Krautkramer and Krautkramer [26]. Shear (G) and bulk (K) elastic moduli were subsequently calculated based on the known relationships for the elastic constants of isotropic solids [1]. The elastic moduli for the 7740 Pyrex™ borosilicate glass was obtained from the literature [27]. Table 3 summarizes the mechanical data. The last column in Table 3 is the ratio of Young's modulus to Vickers hardness, E/H_V, of the glasses.

Results

Vickers hardness

Figure 2 shows the Vickers hardness as a function of temperature for the Float glass and 7740 Pyrex™ borosilicate glass for a maximum load of 1 kgf. The indenter displacement rate was 0.2 μm/s for the Float glass for temperatures up to, and including, 554 °C. For higher temperatures the rate was increased since relaxation of the glass made it impossible for the load to build to 1 kgf. At 585 °C and 606 °C the displacement rate was 0.5 μm/s, while for 630 °C it was 3.5 μm/s. For the Pyrex™ glass the indenter rate was 1.0 μm/s for all tests. Although the data for both glasses are plotted on the same graph, the results are not directly comparable because the indentation rates were different. A 1 μm/s rate was used for the Pyrex™ glass since this rate allowed a 1 kgf load to be reached for all temperatures. The Vickers hardness is seen to decrease continuously for the Float glass. Above the glass transition temperature of the Float glass (~554 °C), the hardness decreases rapidly. For the Pyrex™ glass the hardness remains constant up to 200 °C, followed by a slight increase from 200 °C to 300 °C, which is then followed by a decrease with increasing temperature up to 560 °C. At 570 °C, however, the hardness increased slightly.

In Fig. 3 the Vickers hardness is shown as a function of temperature for glasses OG1, OG2, and OG3. The hardness of all three glasses is seen to decrease with temperature. A load of 200 gf was used for glasses OG1 and OG2, and 100 gf for glass OG3. The indenter displacement rates were 0.2 μm/s for glass OG2, and 0.2 μm/s for glass OG1 for all temperatures except at 500 °C, where a 0.5 μm/s rate was used for the latter. For glass OG3 a 0.5 μm/s rate was used at all temperatures. A higher displacement rate was used for glass OG3 since this glass was softer than the others, and consequently the load had a difficult time increasing at the higher temperatures. Although a 0.2 μm/s rate would allow a 200 gf load to be achieved at lower temperatures for this glass, it was thought better to use the same displacement rate for all temperatures. Temperatures higher than 400 °C resulted in catastrophic failure of the specimen for glass OG2. A 100 gf load was used for glass OG3 since some of the specimens fractured completely in half at the higher temperatures when a 200 gf load was used.

Rate effects on hardness

The effect of the indenter displacement rate on the Vickers hardness of the Float glass at three different temperatures is shown in Fig. 4. At 22 °C there is essentially no effect of the indentation rate on the hardness. At 424 °C there is an initial increase of the hardness as the displacement rate changes from 0.2 μm/s to 1.0 μm/s, but no further change up to 10 μm/s. At 554 °C, i.e., T_g, there is an initial pronounced increase of the hardness with increasing displacement rate, followed by a leveling off. This indicates a strong viscoelastic response of the glass, which is expected near T_g. The hardness values for the 2 kgf tests are slightly lower than the 1 kgf tests, although the difference lessens as the displacement rate increases, such that the values are nearly equal at the 10 μm/s displacement rate. This suggests that at sufficiently high displacement rates, and for temperatures near T_g, the hardness is more influenced by the indenter rate than the maximum load.

Crack length

The crack length around indentation sites was also measured as a function of the temperature. The median-radial cracks were measured from the center of the indentations to the crack tip. Lateral crack sizes were measured from the center of the indentations to a point midway between the median-radial cracks.

Table 3 Mechanical data summary

Glass	H_v (GPa)	K_c (MPa$\sqrt{m}$)	E (GPa)	G (GPa)	K (GPa)	ν	E/H_v
OG1	4.7 ± 0.1	0.78 ± 0.08	63	27	31	0.16	13.4
OG2	8.0 ± 0.3	0.69 ± 0.03	123	48	98	0.29	15.3
OG3	3.6 ± 0.1	0.44 ± 0.02	50	20	33	0.25	13.7
Float	5.3 ± 0.1	0.72 ± 0.02	74	30	44	0.22	14.0
Pyrex™	5.4 ± 0.1	0.76 ± 0.01	63	26	35	0.20	11.7

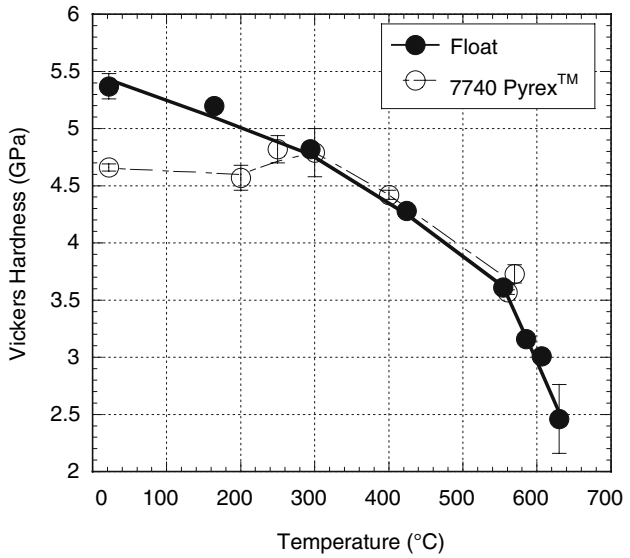

Fig. 2 Vickers hardness as a function of temperature for Float and 7740 Pyrex™ borosilicate glasses. Error bars are ±1 standard deviation of average values. Curves are guides for the eye only

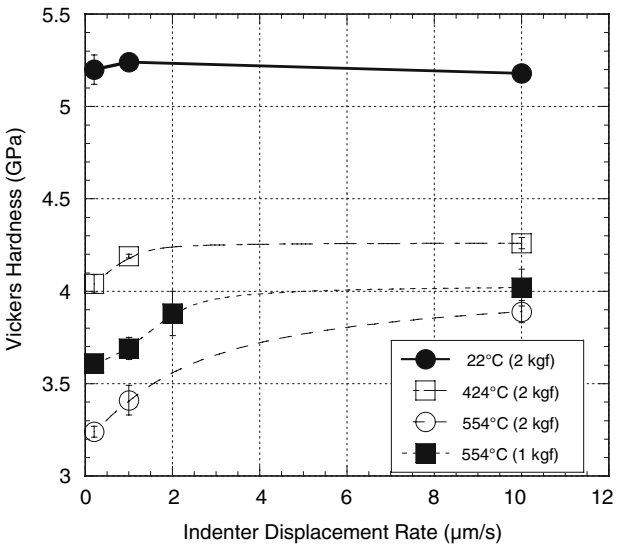

Fig. 4 Vickers hardness of Float glass as a function of indenter displacement rate for several different temperatures. Error bars are ±1 standard deviation of average values. Curves are guides for the eye only

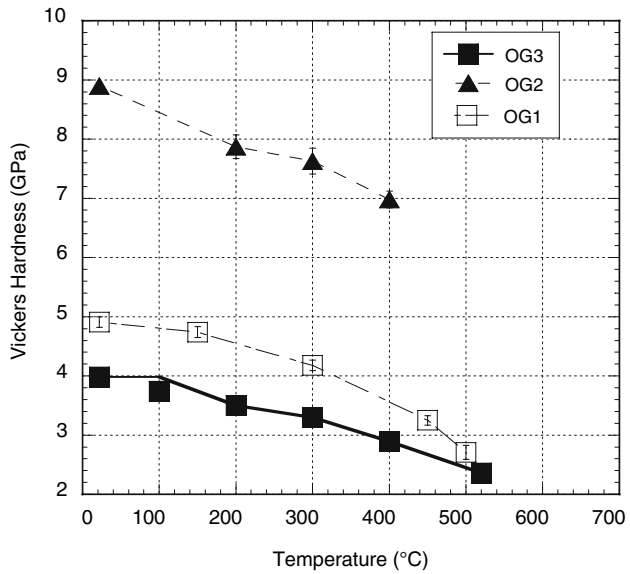

Fig. 3 Vickers hardness as a function of temperature for glasses OG1, OG2, and OG3. Error bars are ±1 standard deviation of average values. Curves are guides for the eye only

In Fig. 5 the median-radial and lateral crack lengths for the Float glass are shown as a function of temperature for 1 kgf maximum load tests. The displacement rate was 0.2 μm/s for temperatures up to and including 424 °C. Higher rates, up to 3.5 μm/s, were used for temperatures above 424 °C. The median-radial crack lengths increased with temperature up to ~424 °C, then decreased with further increases of temperature. In contrast, the lateral crack lengths decreased continuously with increasing temperature. No lateral cracks were observed for temperatures of 554 °C and above. In Fig. 6 the median-radial and lateral crack lengths are shown as a function of temperature for the 7740 Pyrex™ borosilicate glass. A 1 kgf maximum load was used with a 1.0 μm/s displacement rate, for all tests. There was a slight increase of median-radial crack length up to 250 °C, but no change in the lateral crack sizes over this same temperature interval. At 300 °C and above, neither crack type was observed to form. The variation of median-radial and lateral crack sizes for glass OG1 is shown in Fig. 7. A maximum load of 1 kgf was used, with a 1.0 μm/s displacement rate for temperatures up to

300 °C. Above 300 °C rates of 1.5 μm/s and 2.0 μm/s rate were used. The median-radial crack length increased with increasing temperature up to 450 °C (T_g), then decreased thereafter. Above 500 °C no median-radial cracks were observed to initiate for displacement rates up to 10.0 μm/s, with the exception of a single test at 575 °C and 10.0 μm/s rate, in which two median-radial cracks formed. The size of the lateral cracks showed little trend with temperature, as shown in Fig. 7. Above 450 °C no lateral cracks were observed to form for displacement rates up to 10.0 μm/s. Figure 8 shows the variation of median-radial and lateral cracks for glass OG2, for a 1 kgf maximum load. The median-radial crack length increased with increasing temperature. At 400 °C some of the specimens fractured completely, while above this temperature all specimens fractured before the maximum load could be reached. The lateral crack lengths showed little change over the temperature interval. The high-temperature cracking behavior for glass OG3 is shown in Fig. 9. Tests were conducted at maximum loads of 1 kgf and 100 gf, with a 0.5 μm/s displacement rate. The median-radial crack length is seen to increase with temperature for both loads. The increase is more pronounced for the 1 kgf tests. At temperatures above 300 °C, the specimens would completely fracture into two or more pieces at ~500 gf. For the 100 gf tests the specimens did not fail, so tests could be conducted to higher temperatures. After the initial increase in median-radial crack length for the 100 gf tests, a plateau was seen. For tests conducted at temperatures above 500 °C it was difficult to form an indentation in this glass. The lateral crack size for the 1 kgf tests showed a slight decrease in size with temperature.

Load–displacement curves

The load–displacement data for the glasses was plotted for several different temperatures. In Fig. 10 load–displacement curves are shown for the Float glass for 1 kgf maximum load. The displacement rate was 0.2 μm/s for all temperatures shown, except at 606 °C, where a 0.5 μm/s displacement rate was used. This was because the piezoelectric actuator would run out of travel before the load could build to 1 kgf when using a 0.2 μm/s rate. It is seen that both the maximum displacement and residual indentation depth increase with increasing temperature. In addition, the area bound by the loading and unloading portions of each curve, which is indicative of the work of indentation, can be seen to increase with temperature. The very broad curve for the test at 606 °C indicates a highly viscoelastic response. This temperature is well above the glass transition temperature of the Float glass.

Figures 11–14 show load–displacement curves for the other four glasses. Overall, similar behavior occurred as for the Float glass, i.e., an increase of the maximum displacement and residual indentation depth with temperature, along with an increase of the work of indentation. However, load–displacement traces for glass OG2 for temperatures higher than 200 °C tended to be very irregular, and are not shown. This was attributed to slight movement of the samples during testing, possibly because of some unevenness. Another irregularity in a portion of the unloading curve is seen for glass OG3 at a temperature of 520 °C (T_g) in Fig. 14. The slight flattening out of the load–displacement curve may possibly have been due to slight tilting of the sample as the indenter was being removed from the glass surface.

Optical microscopy

Figure 15a–e shows 1 kgf indentation sites in the Float glass as a function of temperature. It can be seen that the median-radial crack traces on the surface increase in length with increasing temperature, however, only up to a point. The length of the surface cracks then decreases starting around 554 °C (T_g). At 630 °C, Fig. 15e, only two small cracks are seen around the indentation, and two of the corners are crack-free. Other indentations at this temperature showed no median-radial cracks. The irregular looking feature present on the upper-right portion of the impression in Fig. 15e was believed to be the result of a piece of material, e.g., furnace insulation or glass, having attached

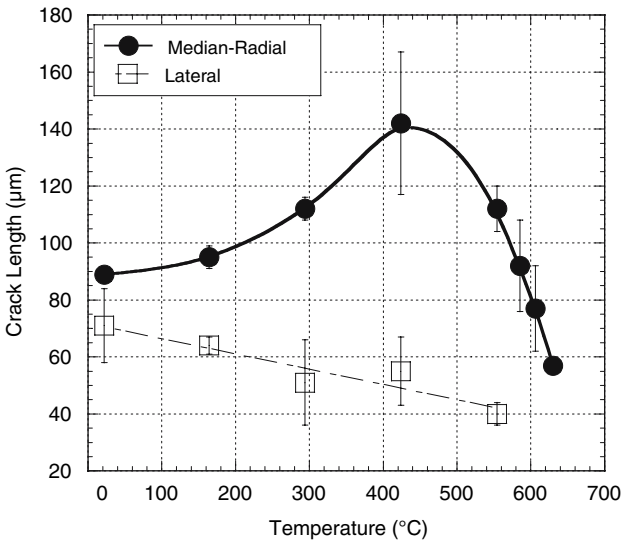

Fig. 5 The variation of median-radial and lateral crack sizes as a function of temperature for the Float glass for 1 kgf maximum load tests. Error bars are ±1 standard deviation of average values. Curves are guides for the eye only

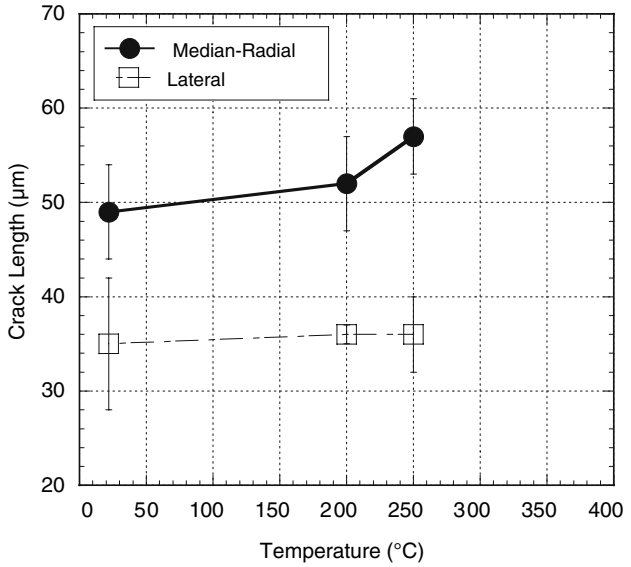

Fig. 6 The variation of median-radial and lateral crack sizes as a function of temperature for the 7740 Pyrex^{TM} borosilicate glass, for 1 kgf maximum load tests. Error bars are ±1 one standard deviation of average values. Curves are guides for the eye only

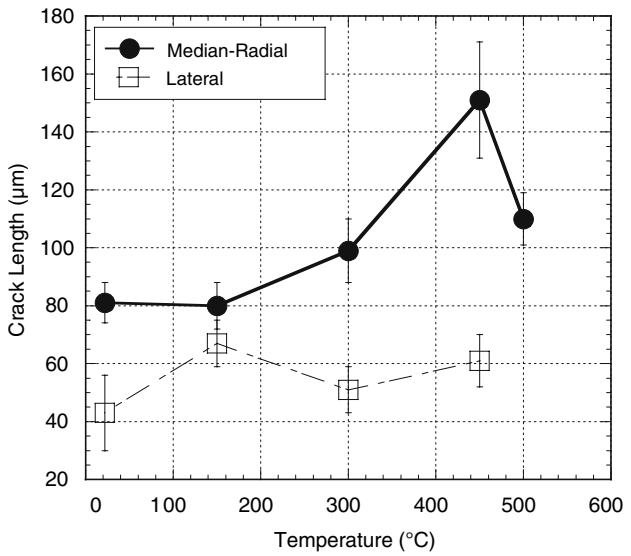

Fig. 7 The variation of median-radial and lateral crack sizes as a function of temperature for glass OG1, for 1 kgf maximum load tests. Error bars are ±1 one standard deviation of average values. Curves are guides for the eye only

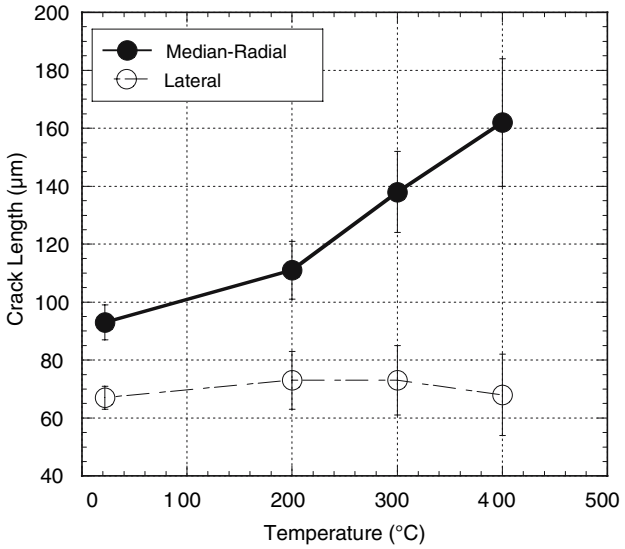

Fig. 8 The variation of median-radial and lateral crack sizes as a function of temperature for glass OG2, for 1 kgf maximum load tests. Error bars are ±1 one standard deviation of average values. Curves are guides for the eye only

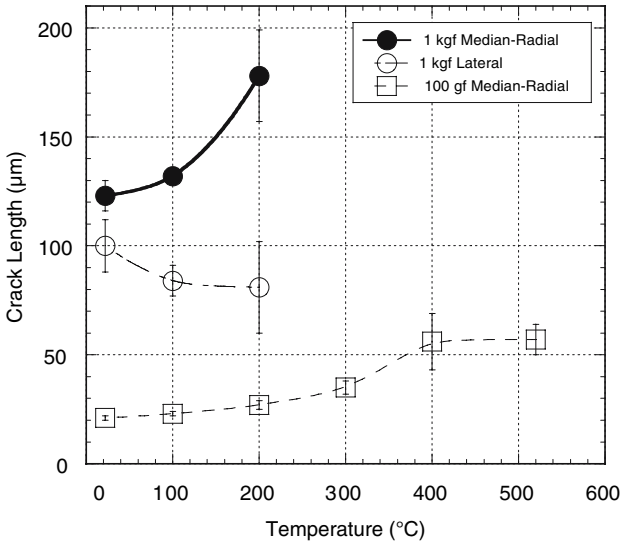

Fig. 9 The variation of median-radial and lateral crack sizes as a function of temperature for glass OG3, for 100 gf and 1 kgf maximum load tests. Error bars are ±1 one standard deviation of average values. Curves are guides for the eye only

itself to the diamond, and upon pressing the diamond into the glass caused the irregular feature. Several other indentations at similar high-temperatures had marks which were identical in shape and location. Subsequent examination of the diamond after testing was complete revealed a small piece of debris on the tip. This piece of debris was removed only by immersing the diamond tip in diluted HF acid (~5% HF) for ~5 min, and hence was most likely a small piece of glass from the sample, or glass fiber from the furnace insulation. Subsequent examination of the diamond under an optical microscope showed no visible changes to the diamond after HF immersion. Massing of the indenter confirmed there was no mass loss compared to the original indenter, which is not surprising since dilute HF acid is not expected to chemically attack diamond. The lateral cracks are seen to decrease in size with increasing temperature in Fig. 15a–c. At 554 °C and above, these cracks were absent, as seen in Fig. 15d, e. Figure 16a and b are

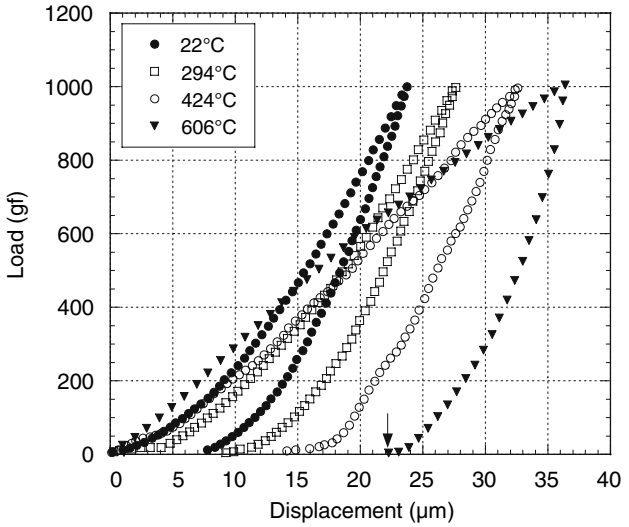

Fig. 10 Load–displacement traces for Float glass at a 1 kgf maximum load for several different temperatures. Arrow indicates the residual penetration depth for the 606 °C test, ~22 μm. Indenter displacement rate was 0.2 μm/s for all tests, except at 606 °C, where a 0.5 μm/s rate was used

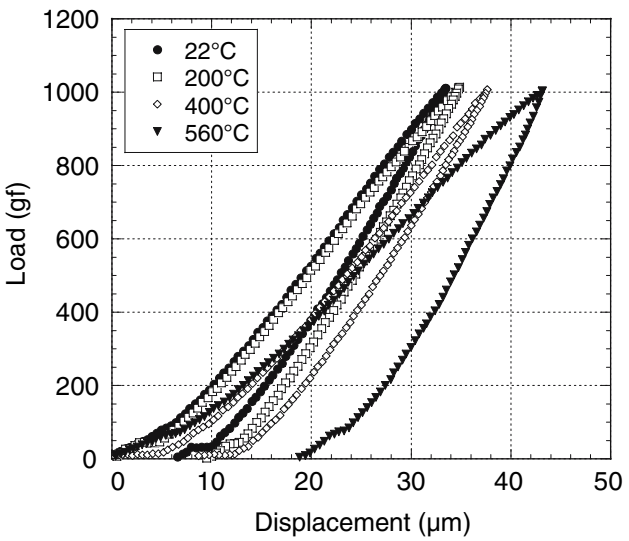

Fig. 11 Load–displacement traces for 7740 Pyrex™ borosilicate glass at a 1 kgf maximum load for several different temperatures. Indenter displacement rate was 1.0 μm/s for all tests

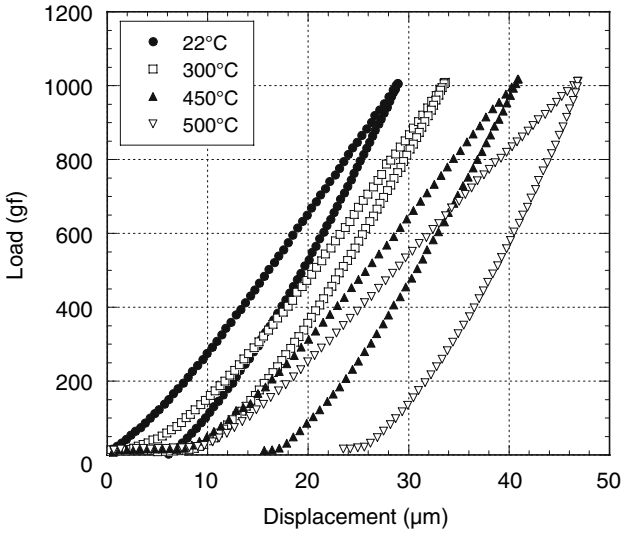

Fig. 12 Load–displacement traces for glass OG1 at a 1 kgf maximum load for several different temperatures. Indenter displacement rate was 1.0 μm/s for tests up to and including 300 °C, and 1.5 μm/s for tests at 450 °C and 500 °C

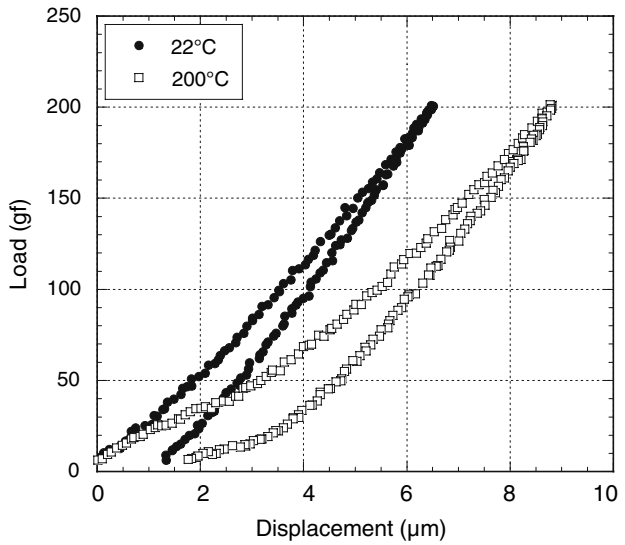

Fig. 13 Load–displacement traces for glass OG2 at a 200 gf maximum load for two different temperatures. Indenter displacement rate was 0.2 μm/s for both tests

high-magnification images of 1 kgf indentation sites formed at 22 °C and 554 °C, respectively. Numerous well-defined shear faults can be seen within the indentation formed at 22 °C, but a clear lack of these is apparent for the indentation formed at 554 °C. Since the shear faults in glass are believed to result from intermittent shear failure of the material at stresses close to the theoretical shear strength [28], it is clear that viscous flow of the Float glass at 554 °C has prevented the stresses from reaching the critical level required for shear failure. The larger size of the indentation formed at 554 °C compared to at 22 °C is obvious as well, and confirms the expectation of lower hardness at high temperature.

In Fig. 17a–d a series of indentation sites for the 7740 Pyrex™ borosilicate glass is shown as a function of temperature. At 22 °C, Fig. 17a, numerous surface ring cracks can be seen surrounding the indentation, but these decreased in number as the temperature was increased to 250 °C, i.e., Fig. 17c. At 560 °C (T_g), Fig. 17d, the surface

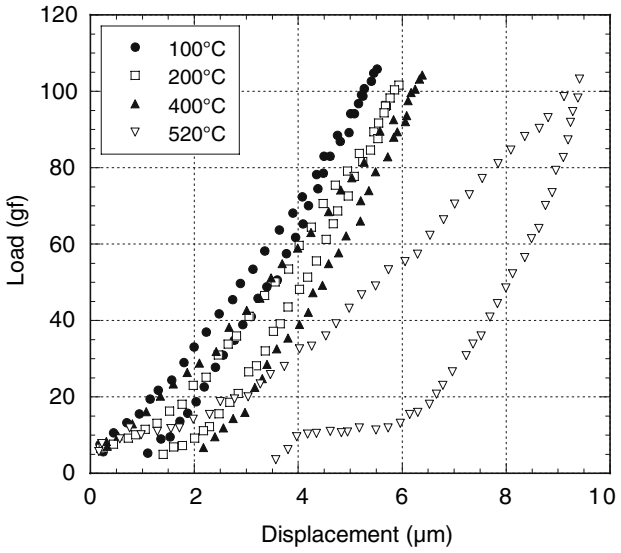

Fig. 14 Load–displacement traces for glass OG3 at a 100 gf maximum load for several different temperatures. Indenter displacement rate was 0.5 μm/s for all tests

ring cracks disappear completely, and the shear faults within the indentation site are not as well defined compared to that at the lower temperatures. The amount of lateral cracking was also seen to diminish with temperature from 22 °C to 250 °C. In addition, at 300 °C and above, no median-radial or lateral cracks formed around the indentations, e.g., Fig. 17d.

Figure 18a–d shows a series of 1 kgf indentation sites in glass OG1, the lead-alkali silicate crown glass, as a function of temperature. At 22 °C surface ring cracks, median-radial cracks, and lateral cracks were present, as seen in Fig. 18a. Surface ring cracks are indicative of an 'anomalous' glass, as discussed by Arora et al. [13]. 'Anomalous' silicate glasses tend to contain relatively high amounts of silica, which gives rise to an open network structure capable of undergoing substantial densification under an indenter.

Densification apparently leads to enhanced surface elastic tensile stresses and the formation of ring-cone cracks. The 7740 Pyrex™ borosilicate glass can also be classified as 'anomalous' because of its densifying behavior, which leads to ring-cone cracking, as shown by Cook and Pharr [14], and by the results in the current work, e.g., Fig. 17a. As the temperature increased the tendency for ring-cone cracking diminished, but the surface length of median-radial cracks began to increase after 150 °C, as seen in Fig. 18b–d. At 300 °C and 450 °C (T_g), Fig. 18c, d respectively, there are no surface ring cracks visible. At 450 °C lateral cracks ceased to form, as seen in Fig. 18d. A higher magnification image of the indentation site at 450 °C is shown in Fig. 18e, and it is apparent that the surface of the indentation contains fewer shear faults compared to indentations made at the lower temperatures. In Fig. 18f and g indentation sites for temperatures of 500 °C and 550 °C are shown, respectively. In order for the load to build to 1 kgf it was necessary to increase the displacement rates to 2.0 μm/s and 3.0 μm/s for the tests at 500 °C and 550 °C, respectively, because the glass becomes increasingly more viscoelastic. Slower displacement rates resulted in the piezoelectric actuator running out of displacement before the load reached 1 kgf. A ring crack, which extends half way around the indentation, can be seen in Fig. 18f. The higher displacement rate may have caused the glass to behave slightly more elastic, thus enabling higher surface elastic tensile stresses to build, resulting in ring cracking. However, no lateral cracks were formed, and the median-radial cracks which initiated were shorter in length compared to at 450 °C. In addition, only three of the four corners had median-radial cracks. The indentation at 550 °C, Fig. 18g, contained no median-radial or lateral cracks, and virtually no shear faults, although a small and incomplete surface ring crack, which is mostly contained within the indentation, is visible.

Figure 19a–d shows indentation sites for glass OG2 over the temperature range 22–400 °C, respectively. The images show clearly the increase in the surface length of the median-radial cracks with increasing temperature. At 400 °C some of the specimens fractured completely into two or more pieces before reaching the desired load, due to the extension of the cracks through the specimen thickness. Additional tests were conducted at temperatures of 600 °C and 642 °C (T_g) but the specimens fractured even more readily. Tests were not conducted above 642 °C for fear of causing oxidation of the diamond indenter.

Figure 20a–d shows indentation sites for glass OG3 over the temperature range 22–550 °C. Similar to glass OG2, the surface length of the median-radial cracks is seen to increase with increasing temperature. At 300 °C and above, most of the specimens fractured in half before the load could reach 1 kgf. For this reason, tests were conducted at 100 gf for temperatures of 520 °C (T_g), and 200 gf at 550 °C. These tests are shown in Fig. 20e and f, respectively. At 520 °C radial cracks are clearly seen around the indentation site, but at 550 °C these cracks, and the indentation, are barely visible. In addition, no lateral cracks are seen around the indentation in Fig. 20e. A 200 gf load was used at 550 °C because a 100 gf load did not produce any visually detectable indentation. The indentation in Fig. 20f is barely visible as a small bright region, and three median-radial cracks extending from this region are just visible. Some healing of the crack surfaces may have occurred at this high temperature, thus making the cracks less visible.

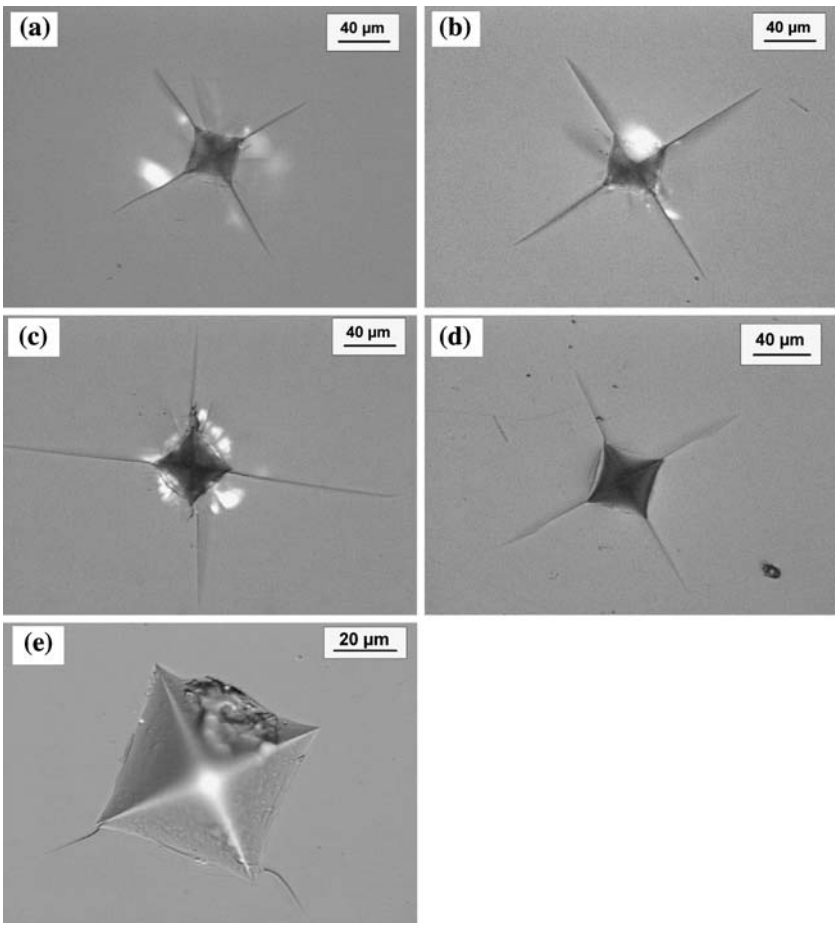

Fig. 15 Vickers indentation sites in Float glass for several different temperatures and 1 kgf maximum load: (**a**) 22 °C, (**b**) 294 °C, (**c**) 424 °C, (**d**) 554 °C, and (**e**) 630 °C. Indenter displacement rate was 0.2 μm/s for all tests, except at 630 °C, where a 3.5 μm/s rate was used. Original magnification was 250× (**a**–**d**) and 625× (**e**). Images from reflected light optical microscopy with differential interference contrast (**a**–**d**) and brightfield (**e**) conditions

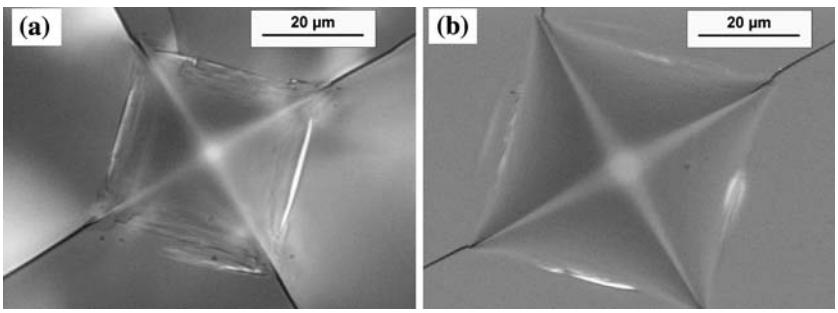

Fig. 16 High-magnification images of 1 kgf Vickers indentation sites in Float glass formed at (**a**) 22 °C and (**b**) 554 °C. Image in (**b**) is from the same indentation site shown in Fig. 15d. Original magnification was 1,000× (**a**–**b**). Images from reflected light optical microscopy with brightfield conditions

Displacement rate effects on crack morphology

Additional tests for the Float glass were conducted where the displacement rate was changed while keeping the temperature and maximum load constant. For example, 2 kgf indentation sites made at rates of 0.2 μm/s and 10.0 μm/s at 554 °C (T_g) are shown in Fig. 21a and b, respectively. Whereas no lateral cracks formed around the indentation site at 0.2 μm/s, extensive lateral crack development occurred for the indentation site formed at 10.0 μm/s. Transmitted light images of the same indentation sites, shown in Fig. 21c, d, reveal further differences. The indentation formed at 10.0 μm/s contains numerous smaller splinter like cracks; however, these are absent in the indentation formed at 0.2 μm/s. These differences can be attributed to the fact that the glass is viscoelastic at the glass transition temperature, and hence the magnitudes of the stresses which build are rate dependent. Recall the hardness of the Float glass increased with increasing displacement rate at this temperature and load, i.e., Fig. 4. The load–displacement curves responsible for producing these indentation sites are shown in Fig. 22. It is clear that the faster rate of loading enabled the maximum load to be reached at a shallower penetration depth. In addition, the

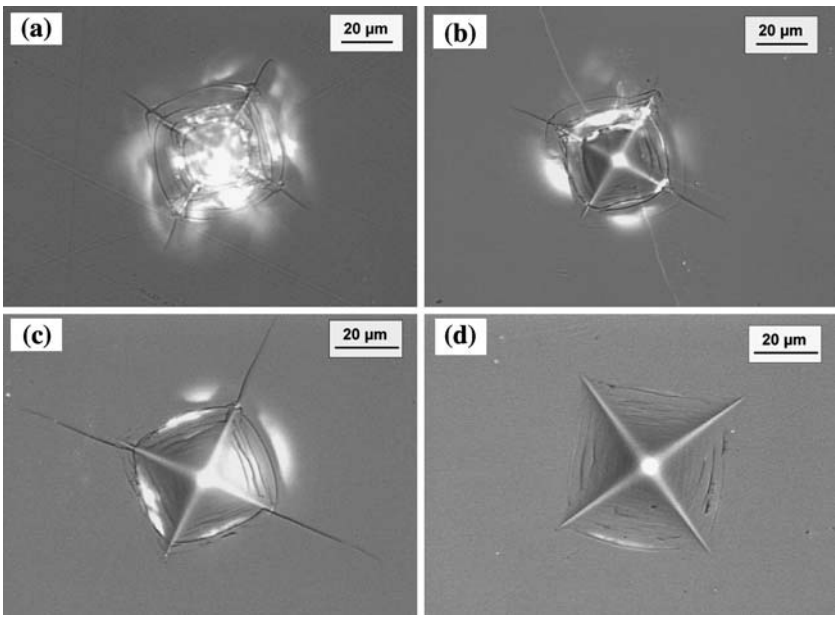

Fig. 17 Vickers indentation sites in 7740 Pyrex™ borosilicate glass for several different temperatures and 1 kgf load: (**a**) 22 °C, (**b**) 200 °C, (**c**) 250 °C, and (**d**) 560 °C. Indenter displacement rate was 1.0 μm/s for all tests. Original magnification was 500× (**a**, **b**) and 625× (**c**, **d**). Images from reflected light optical microscopy with brightfield conditions

hysteresis and permanent indentation depth are much smaller for the faster loading rate, indicating less consumed energy and a smaller indentation size, respectively.

Discussion

Hardness

The continuous decrease in hardness with increasing temperature for the Float glass, and glasses OG1, OG2, and OG3, is consistent with a weakening of the glass structure with increasing temperature. Yamane and Mackenzie [29] analytically derived an equation for calculating the Vickers hardness of silicate and non-silicate glasses. They proposed that the resistance of a glass to permanent indentation is a combination of resistances to shear flow, elastic deformation, and densification. According to Yamane and Mackenzie the resistance to shear flow is governed by the shear modulus and a relative bond strength factor, while that of elastic deformation by the bulk modulus.

Resistance to densification is a combination of resistance to both elastic deformation and shear. The equation derived by them, $H_V = 0.19(\alpha GK)^{1/2}$, where G and K are shear and bulk moduli, respectively, and α is the relative bond strength factor, thus predicts decreased Vickers hardness with decrease of the elastic moduli and bond strength. Excellent agreement between calculated and measured values were obtained by Yamane and Mackenzie on a wide range of glasses. Work by Spinner [30] has shown that the Young's modulus and shear modulus of many silicate glasses decreases continuously with increasing temperature, while the Poisson's ratio increases slightly. The bulk modulus also decreased with temperature, since for isotropic materials the bulk modulus is directly proportional to Young's modulus (E), and only weakly dependent on Poisson's ratio. In addition, work by Shinkai et al. [31] shows that both the Young's and shear modulus decrease continuously with increasing temperature for Float glass. The decrease in the elastic moduli was relatively small up to 300 °C, but above this temperature the decrease was rapid and substantial, particularly for the Young's modulus. Thus, the decrease in hardness of the Float, OG1, OG2, and OG3 glasses is likely a result of the decrease in the shear and bulk moduli of the glasses with increasing temperature. Glasses which have negative dependencies of elastic moduli with temperature, but positive dependencies on pressure, are termed 'normal,' since most glasses display this behavior [32]. Glasses with the opposite characteristics are termed 'anomalous.' 'Normal' glasses tend to contain substantial amounts of modifier ions which break-up the network structure, whereas 'anomalous' glasses contain little or no modifier ions [32]. Vitreous silica is the prototypical 'anomalous' glass. The 7740 Pyrex™ borosilicate glass is 'anomalous' in that the elastic moduli initially increase with temperature up to about 450 °C, where further increases of temperature cause the elastic moduli to decrease, as shown by Spinner [30]. This behavior may account for the slight increase of the hardness from 22 °C to 300 °C for this glass (recall Fig. 2). Since Young's modulus is proportional to the slope of the interatomic force-separation curve at the equilibrium spacing, and to the equilibrium bond length spacing itself, r_o, i.e., $E \approx (1/r_o)(dF/dr)_{r=r_o}$ [33] any increase of the

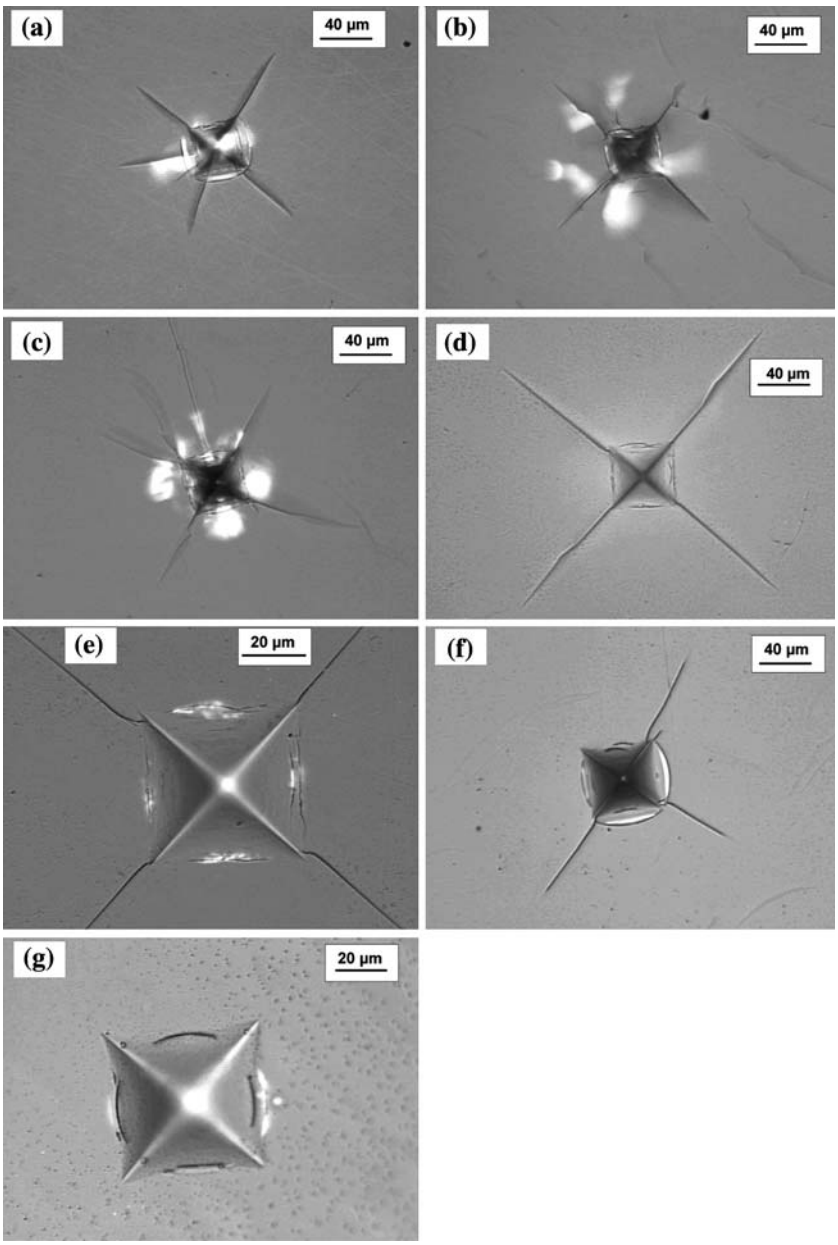

Fig. 18 Vickers indentation sites in glass OG1 for several different temperatures and 1 kgf load: (**a**) 22 °C, (**b**) 150 °C, (**c**) 300 °C, (**d**) 450 °C, (**e**) higher magnification image of (**d**), (**f**) 500°C, and (**g**) 550°C. Indenter displacement rate was 1.0 μm/s for (**a**–**c**), 1.5 μm/s for (**d**, **e**), 2.0 μm/s for (**f**), and 3.0 μm/s for (**g**). Original magnification was 250× (**a**–**d**, **f**), 625× (**e**), and 500× (**g**). Images from reflected light optical microscopy with brightfield conditions

interatomic spacing such as that caused by thermal expansion as a result of heating, would be expected to decrease Young's modulus, and hence G and K, and hence hardness. A decrease in the slope of the force-separation curve at r_o would also cause the elastic moduli to decrease.

Viscoelasticity

A material is said to be viscoelastic if it exhibits both viscous (time-dependent) and elastic (time-independent) behavior to a mechanical stimulus [34]. Glass behaves viscoelastic in the glass transformation range [1]. In an elastic body the strains and stresses build up, and are removed, instantaneously. Hooke's law governs the behavior of elastic bodies, where the stress is linearly related to the strain. For the case of an applied shear stress, $\tau = G\varepsilon$, where τ is shear stress, G is shear modulus, and ε is shear strain. In a viscous body, however, the stress that builds is not a function of the strain, but of the strain rate. That is, the stress is time-dependent. For viscous materials subjected to low shear stress, Newton's law of viscosity holds i.e., $\tau = \eta\dot{\varepsilon}$, where η is the coefficient of viscosity and $\dot{\varepsilon}$ is the shear strain rate. For viscoelastic materials the Maxwell model is often used to represent the behavior, and consists of an elastic spring and viscous dashpot connected in series. For this situation the following equation is known to hold [34]:

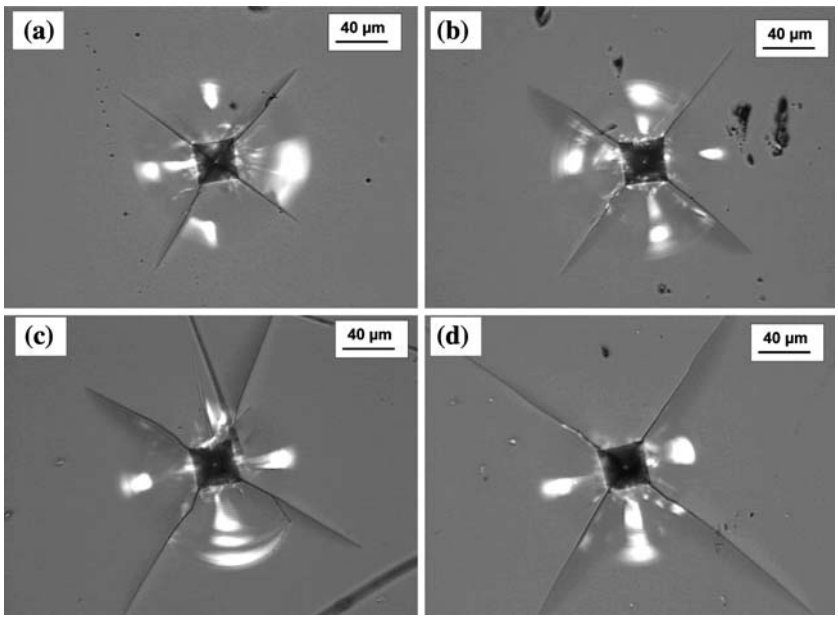

Fig. 19 Vickers indentation sites in glass OG2 for several different temperatures and 1 kgf load: (**a**) 22 °C, (**b**) 200 °C, (**c**) 300 °C, and (**d**) 400°C. Indenter displacement rate was 1 μm/s for all tests. Original magnification was 250× for (**a–d**). Images from reflected light optical microscopy with brightfield conditions

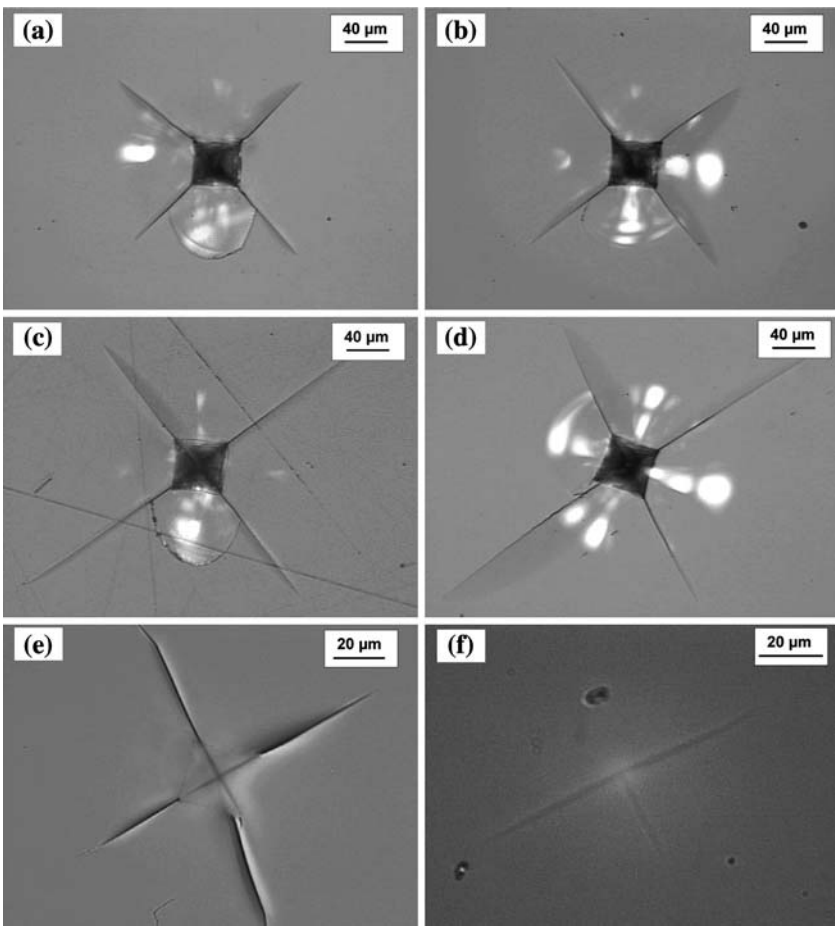

Fig. 20 Vickers indentation sites in glass OG3 for several different temperatures: (**a**) 22 °C, (**b**) 100 °C, (**c**) 200 °C, (**d**) 300 °C, (**e**) 520 °C, and (**f**) 550 °C. Maximum load was 1 kgf (**a–d**), 100 gf (**e**), and 200 gf (**f**). Indenter displacement rate was 0.5 μm/s for all tests. Original magnification was 200× (**a–d**), 500× (**e**), and 625× (**f**). Images from reflected light optical microscopy with differential interference contrast (**a–d**), and transmitted light optical microscopy with brightfield conditions (**e–f**)

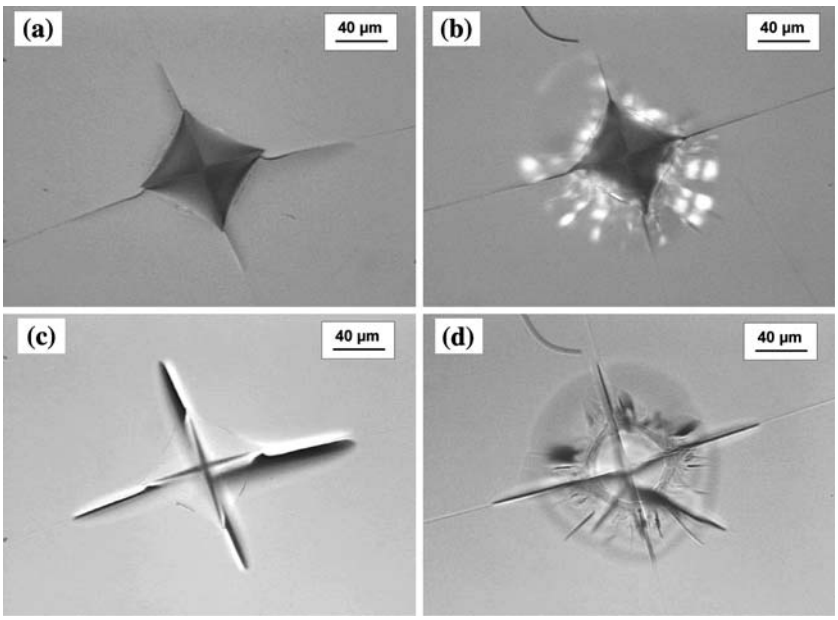

Fig. 21 Vickers indentation sites in Float glass made at 554 °C and 2 kgf load at (**a**) 0.2 μm/s and (**b**) 10.0 μm/s displacement rates. Transmitted light images of same indentations sites are shown in (**c**, **d**), and correspond to images in (**a**, **b**), respectively. Original magnification was 250× (**a**–**d**). Images from reflected light optical microscopy with differential interference contrast (**a**, **b**), and transmitted light optical microscopy (**c**, **d**)

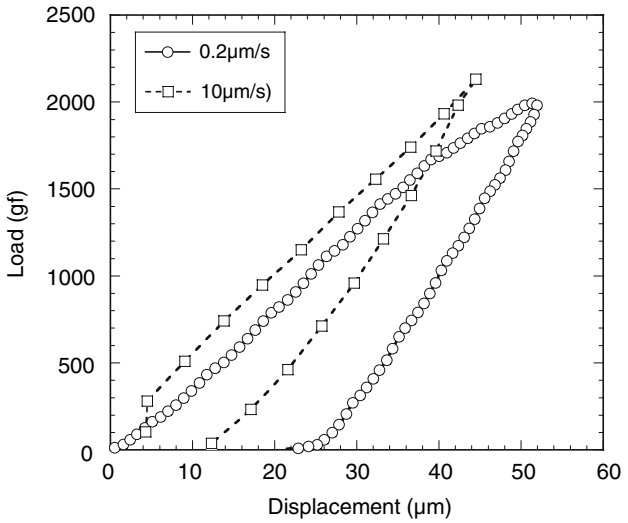

Fig. 22 Load–displacement curves, corresponding to the indentation sites shown in Fig. 21, illustrating the viscoelastic behavior of the Float glass specimen at the glass transition temperature (~554 °C)

$$\frac{d\varepsilon}{dt} = \frac{1}{E}\frac{d\sigma}{dt} + \frac{\sigma}{\eta} \tag{3}$$

For the indentation tests in the current work the displacement rate for a given run was constant, and hence to a first approximation this may be considered to be analogous to a constant strain rate. Hence, $d\varepsilon/dt$ in Eq. 3 may be considered to be zero. Solving this differential equation then yields the stress as a function of both time and material properties:

$$\sigma = \sigma_o \exp\left(\frac{-tE}{\eta}\right) \tag{4}$$

where σ = stress; σ_o = pre-exponential constant = $E\varepsilon$; t = time; E = Young's modulus; and η = viscosity.

Although Eq. 4 strictly applies only to a uniaxial tension or compression test, to a first approximation it can be applied to explain some of the indentation results, where at least part of the stress is compressive. For example, the increase of the hardness of the Float glass with increasing displacement rate for temperatures near and at the glass transition temperature (see Fig. 4), can be attributed to a decrease of the time, t, in Eq. 4. Decreasing the contact time, t, would cause the stress to increase due to less time available for viscous flow, consistent with the increase of hardness (mean contact stress) with increase of the displacement rate. Recall that increasing the displacement rate decreases the total indenter contact time for a given maximum load. The rate effect is not as pronounced at 424 °C (Fig. 4) compared to at T_g, where the glass is more viscoelastic. For an instantaneous contact, i.e., $t = 0$, Eq. 4 yields $\sigma = \sigma_o = E\varepsilon$, i.e., elastic behavior results. Also, for temperatures well removed from the glass transition temperature, the relaxation time is extremely large. The relaxation time, t_R, which represents the time needed for the initial stress to decrease by ~63%, is given by η/E, and thus Eq. 4 can also be represented as:

$$\sigma = \sigma_o \exp\left(\frac{-t}{t_R}\right) \tag{5}$$

With increasing temperature the viscosity decreases, and so does E. However, the viscosity decreases faster, and hence the relaxation time decreases with increasing temperature. Thus, there is essentially no rate dependence of hardness at 22 °C for the Float glass, since the relaxation time is

extremely large compared to the time of the test. At 424 °C the relaxation time is not as large, and hence the contact time (displacement rate) begins to have some influence on the hardness, as seen in Fig. 4. At 554 °C the relaxation time is even smaller, and hence the rate effects are even more pronounced. The load is also seen to have an effect at this temperature as well. The 2 kgf tests required a longer contact time to reach this load, hence the glass had more time to relax, resulting in the lower hardness values compared to the 1 kgf tests (see Fig. 4). Thus, the overall contact time is equally important as the contact rate in influencing the viscous flow under a sharp indenter. The near leveling off of the hardness with increasing displacement rate seen at 424 °C and 554 °C (Fig. 4) indicates a constant flow stress limit is possibly being reached, and resembles that of shear-rate thinning (pseudoplastic) behavior. This may be due to a structural change in the glass which helps to facilitate flow at high displacement rates.

The increase of the hardness with increasing displacement rate also explains the difference in the cracking behavior between the two indentation sites shown in Fig. 21. Since the stress beneath a sharp indentation is expected to scale with the hardness [35], the increased cracking around the indentation made at 10.0 μm/s is consistent with the higher hardness measured at this rate compared to at 0.2 μm/s (see Fig. 4). In addition, the load–displacement traces for these indentation sites, shown in Fig. 22, show the faster rate test to undergo less penetration and have a smaller hysteresis loop compared to the slower rate test, indicative of viscoelastic behavior of the glass at this temperature. The area within the hysteresis loop represents the energy consumed in forming the indentation and any cracks. The energy consumed in forming the indentation may include that used to densify the glass, create shear faults, and push material out of the way, in addition to any residual elastic strain energy stored in the glass after the test is complete. Whereas ~73% elastic depth recovery was observed for the 10.0 μm/s test, only ~52% was observed for the 0.2 μm/s test.

Cracking behavior

Median-radial cracks

For all glasses, the length of median-radial cracks around the indentation sites increased with initial increases of temperature, although the increase for the Pyrex™ glass was only slight. The following expression, after Anstis et al. [24], relates the crack length around Vickers indentations in ceramics and glasses to the material properties and hardness:

$$c = \left\{ 0.016 \frac{(\chi_r)^{1/2} F}{K_c} \right\}^{2/3} \tag{6}$$

where c = crack length (measured from center of indentation to crack tip); χ_r = residual crack driving 'force' = E/H); F = indentation load; and K_c = indentation fracture toughness.

Thus, Eq. 6 predicts that for constant indentation load the crack length should increase with either an increase of χ_r, or a decrease in toughness. The term χ_r is the residual crack driving 'force,' or motive, and is given by E/H. Materials with high E/H are termed 'soft,' and the ratio of the 'plastic' zone volume to the indentation volume tends to be high. From Table 3 it is seen that glasses OG2 and OG3 have relatively high E/H, 15.3 and 13.7, respectively, and these were also the glasses that failed abruptly when tested at high temperature under moderate loads. Although the E/H for glass OG3 is slightly smaller than for Float glass (14.0), the toughness of the former is considerably less, enabling cracks to propagate much further compared to Float glass, thus causing the catastrophic failure. Although E is expected to decrease with increasing temperature for all the glasses examined, except the 7740 Pyrex™ borosilicate, the hardness decreases faster, and hence χ_r is expected to increase with initial increases of temperature. As shown by Shinkai et al. [31] and Wiederhorn et al. [32], the fracture toughness of Pyrex™ borosilicate glass, Float glass, and vitreous silica undergo little to no change for initial increases of temperature. For the borosilicate glass the fracture toughness showed little change up to ~600 °C, and for vitreous silica no change up to ~800 °C. Above 800 °C the toughness of the vitreous silica began to increase. For the Float glass no change in fracture toughness was observed up to ~350 °C [31]. However, the fracture toughness decreased between 350 °C and 550 °C, followed by an increase at >550 °C. Therefore, the increase of the median-radial crack length with initial increase of temperature is most likely a result of the increase in crack driving force, χ_r, due to the more rapid decrease of hardness compared to Young's modulus of the glasses. For the Float glass, a decrease in the fracture toughness most likely contributes to the increased crack length as well. The plane-strain fracture toughness can be expressed as [36]:

$$K_{Ic} = \left(\frac{2E\gamma_f}{1 - \nu^2} \right)^{1/2} \tag{7}$$

where γ_f is the fracture surface energy and ν is Poisson's ratio. If this expression for K_{Ic} is substituted for K_c in Eq. 6, the Young's modulus (E) drops out of the expression. Thus, the crack length is seen to be influenced by a fundamental material property, i.e., the fracture surface energy.

Therefore, the fracture surface energy is likely to decrease for the Float glass as the temperature is initially increased, which would help increase the crack length. The same could be said for the other glasses, with the possible exception of the Pyrex™ glass. For the Pyrex™ borosilicate glass, the increase of the Young's modulus with temperature would presumably further increase the crack driving force, viz., Eq. 4. However, the fact this glass tends to densify under an indenter [13, 14], and have relatively high fracture toughness, leads to crack lengths that are smaller compared to the other glasses examined (recall the crack length increased only a small amount with temperature for this glass, followed by a cessation of crack formation). In addition, this glass had the smallest E/H value of all the glasses examined, further supporting this concept (see Table 3). The catastrophic failure observed for glasses OG2 and OG3 at temperatures below their glass transition temperatures (section "Crack length"), is attributed to the growth of the median-radial cracks through the thickness of the specimens. These glasses had relatively sharp increases of median-radial crack length with temperature (1 kgf tests), which means the fracture resistance of these glasses is more sensitive to changes in temperature than the other glasses.

The decrease of the median-radial crack lengths for temperatures approaching, and above T_g, can be attributed to increased viscous flow relieving the crack driving force, and crack tip stress. Viscous flow, as opposed to fracture, becomes the dominant material response at these temperatures. At these high temperatures the decrease in Young's modulus becomes significant, possibly causing a decrease in E/H, and thus a reversal in the crack length vs. temperature behavior. For the Pyrex™ glass, median-radial cracks ceased forming at 300 °C, which is considerably below it glass transition temperature ($\sim$560 °C). However, this may be due to its 'anomalous,' i.e., densifying behavior, which tends to further reduce the crack driving force [13]. In addition, examination of the indentation site in Fig. 17d shows that the shear faults are not as severe compared to that at lower temperatures. Since the shear faults, and intersection of faults, are the most likely nucleation sites for cracks [28, 37, 38], a decrease in the severity of these faults would make crack initiation more difficult.

Lateral cracks

Unlike the median-radial cracks, the sizes of the lateral cracks either did not change, or decreased with increase of temperature. In addition, for the Float glass and glass OG1, lateral cracks ceased to form at temperatures considerably lower than the temperatures at which the median-radial cracks ceased to form.

The noticeable decrease in the lateral crack lengths with temperature for the Float glass indicates that the crack driving force for these cracks decreases with temperature, including the initial temperature range where the median-radial cracks are seen to increase. Since lateral cracks tend to form near complete unloading of the indenter [13, 14, 21], after the median-radial cracks, it appears that most of the driving force is consumed by the growth of the median-radials, leaving proportionally less available for lateral crack extension with increasing temperature. In addition, since lateral cracks form later in time than median-radial cracks, a greater amount of stress relaxation has taken place by the time the lateral cracks initiate, at least for temperatures near T_g, and this would further reduce the crack driving force. This would also help to explain why lateral cracks ceased to form at temperatures considerably less than the temperatures at which median-radial cracks ceased to form, as observed for the Float and OG1 glasses. It is believed this would also have been observed in glasses OG2 and OG3 had the samples been made thicker to avoid the through-thickness median-radial cracking observed at the higher temperatures. Glass OG3 showed a similar trend with the lateral cracks lengths as the Float glass, however, the Pyrex™ borosilicate and OG2 glasses showed a more-or-less invariance of lateral crack size with temperature. For these glasses the lateral cracks did not form uniformly around the indentations at the higher temperatures, e.g., see Figs. 17c and 19c, d, indicating an overall diminishing crack nucleation and extension force.

Summary

The Vickers indentation behavior of five commercial glasses was investigated as a function of temperature using a recording microindentation instrument. The hardness was observed to decrease continuously with temperature for all glasses, with the exception of the 7740 Pyrex™ borosilicate glass, where the hardness remained nearly constant up to $\sim$300 °C, followed by a decrease with increasing temperature. The decrease in hardness of the glasses is attributed to a decrease of the elastic moduli and bond strength with increasing temperature. The 'anomalous' behavior of the elastic moduli for the 7740 Pyrex™ borosilicate glass helped prevent the hardness from decreasing for initial temperature increases. However, further increases of temperature caused the hardness to decrease. The lengths of median-radial cracks increased considerably with temperature for temperatures below the glass transition temperature for all glasses, with the exception of the Pyrex™ borosilicate glass, where only a slight increase was seen. The increase of crack length is attributed to an increase in the residual crack driving force (E/H) with increasing temperature, due to a reduction in

hardness, and a decrease in the fracture surface energy of the glasses as well. The decrease in crack length observed for the Float glass and glass OG1 for temperatures near and above T_g is attributed to viscous flow, which reduces the crack driving force and crack tip stress. If the catastrophic failure of glasses OG2 and OG3 above T_g could have been avoided, it is believed that similar behavior would have resulted. Viscoelastic behavior of the Float glass was apparent as an increase of the hardness, and severity of cracking, with increasing indenter displacement rate for temperatures near and at T_g.

Acknowledgement The authors are grateful for financial support provided by the National Science Foundation Industry-University Center for Glass Research at Alfred University.

References

1. Varshneya AK (1994) Fundamentals of inorganic glasses. Academic Press, San Diego, CA
2. Shelby JE (1997) Introduction to glass science and technology. The Royal Society of Chemistry, Cambridge, UK
3. Griffith AA (1920) Philos Trans R Soc London 221:163
4. Mueller DW, Mylchreest GD (1947) In: American Ceramic Society Glass Division Autumn Meeting Presentation (1947) Abstract in Glass Ind 28(10):515
5. Shand EB (1954) J Am Ceram Soc 37(2):52
6. Budd SM, Cowan ND, Bourne R (1980) J Non-Cryst Solids 38&39:409
7. Wiederhorn SM, Lawn BR (1979) J Am Ceram Soc 62(1–2):66
8. Lawn BR, Marshall DB, Wiederhorn SM (1979) J Am Ceram Soc 62(1–2):71
9. Lawn BR, Fuller ER, Wiederhorn SM (1976) J Am Ceram Soc 59(5–6):193
10. Lawn BR, Wiederhorn SM, Johnson HH (1975) J Am Ceram Soc 58(9–10):428
11. Varner JR, Hallwig W, Walter A (1980) J Non-Cryst Solids, 38&39:413
12. Ritter JE Jr, Strzepa P, Jakus K (1984) Phys Chem Glasses 25(6):159
13. Arora A, Marshall DB, Lawn BR (1979) J Non-Cryst Solids 31(3):415
14. Cook RF, Pharr GM (1990) J Am Ceram Soc 73(4):787
15. Lawn BR, Wilshaw TR (1975) J Mater Sci 10(6):1049
16. Wiederhorn SM, Hockey BJ (1980) J Non-Cryst Solids 38&39:433
17. Westbrook JH (1960) Phys Chem Glasses 1(1):32
18. Keulen NM, Dissel M (1993) Glass Technol 34(5):200
19. Le Bourhis E, Metayer D (2000) J Non-Cryst Solids 272:34
20. Michel MD, Mikowski A, Lepienski CM, Foerster CE, Serbena FC (2004) J Non-Cryst Solids 348:131
21. Wilantewicz TE, Varner JR (2001) In: Varner JR, Quinn GD (eds) Fractography of glasses and ceramics IV. American Ceramic Society, Westerville, OH, pp 433–450
22. Lu FX, Liu JM, Chen GC, Tang WZ, Li CM, Song JH, Tong YM (2004) Diamond Relat Mater 13(3):533
23. "Standard Test Method for Microhardness of Materials," ASTM Standard E 384-89 (1990) Annual book of ASTM standards, vol 3.01. American Society for Testing and Materials, West Conshohocken, PA
24. Anstis GR, Chantikul P, Lawn BR, Marshall DB (1981) J Am Ceram Soc 64(9):533
25. Wiederhorn SM (1983) J Am Ceram Soc 52(2):99
26. Krautkramer J, Krautkramer H (1977) Ultrasonic testing of materials, 2nd edn. Springer-Verlag, Berlin, Germany
27. Schneider SJ (ed) (1991) In: Ceramics and glasses. Engineered materials handbook, vol 4. American Ceramic Society, Westerville, OH
28. Lawn BR, Dabbs TP, Fairbanks CJ (1983) J Mater Sci 18(9):2785
29. Yamane M, Mackenzie JD (1974) J Non-Cryst Solids 15:153
30. Spinner S (1956) J Am Ceram Soc 39(3):113
31. Shinkai N, Bradt RC, Rindone GE (1981) J Am Ceram Soc 64(7):426
32. Wiederhorn SM, Johnson H, Dines AM, Heuer AH (1974) J Am Ceram Soc 57(8):336
33. Makishima A, Mackenzie JD (1973) J Non-Cryst Solids 12:35
34. Green DJ (1998) An introduction to the mechanical properties of ceramics. Cambridge University Press, Cambridge, UK
35. Lawn BR, Evans AG (1977) J Mater Sci 12(11):2195
36. Lawn BR (1993) Fracture of brittle solids, 2nd edn. Cambridge University Press, Cambridge, UK
37. Hagan JT, Swain MV (1978) J Phys D: Appl Phys 11:2091
38. Hagan JT (1980) J Mater Sci 15(6):1417